JOURNAL OF APPLIED PHYSICS 115, 123711 (2014)

Two dimensional electron transport in modulation-doped $In_{0.53}Ga_{0.47}As/AlAs_{0.56}Sb_{0.44}$ ultrathin quantum wells

Cheng-Ying Huang,[1,a)] Jeremy J. M. Law,[1] Hong Lu,[1,2] Debdeep Jena,[3] Mark J. W. Rodwell,[1] and Arthur C. Gossard[1,2]
[1]*Department of Electrical and Computer Engineering, University of California, Santa Barbara, California 93106, USA*
[2]*Materials Department, University of California, Santa Barbara, California 93106-5050, USA*
[3]*Department of Electrical Engineering, University of Notre Dame, Notre Dame, Indiana 46556, USA*

(Received 17 December 2013; accepted 13 March 2014; published online 31 March 2014)

We have investigated the growth and electron transport in $In_{0.53}Ga_{0.47}As/AlAs_{0.56}Sb_{0.44}$ two dimensional electron gases (2DEG) and compared their properties with $In_{0.53}Ga_{0.47}As/In_{0.52}Al_{0.48}As$ 2DEGs. For 10 nm thick InGaAs wells, the electron mobility of InGaAs/AlAsSb 2DEGs is comparable to that of InGaAs/InAlAs 2DEGs. Upon thinning the wells to 3 nm, the 2DEG mobility is degraded quickly and stronger interface roughness scattering is observed for InGaAs/AlAsSb heterointerfaces than for InGaAs/InAlAs heterointerfaces. Changing the group-V exposure between As and Sb during growth interruptions at the InGaAs/AlAsSb interfaces did not significantly change the 2DEG mobility. With the insertion of a two monolayer InAlAs at the InGaAs/AlAsSb interfaces, the interface roughness scattering is reduced and the mobility greatly increased. The room temperature 2DEG mobility shows 66% improvement from 1.63×10^3 $cm^2/V{\cdot}s$ to 2.71×10^3 $cm^2/V{\cdot}s$ for a 3 nm InGaAs well. © *2014 AIP Publishing LLC*. [http://dx.doi.org/10.1063/1.4869498]

I. INTRODUCTION

High electron mobility InGaAs channels have recently been extensively studied as a potential replacement of Si channels for future generations of VLSI technology.[1–6] The potential for increased on-state current using InGaAs channel relies on the superior transport properties of two dimensional electron gases (2DEG), which is manifested by higher carrier mobility and higher ballistic injection velocities. Recently, $AlAs_{0.56}Sb_{0.44}$, with higher conduction band offset to $In_{0.53}Ga_{0.47}As$ than $In_{0.52}Al_{0.48}As$ ($X_{AlAsSb} - \Gamma_{InGaAs} \sim 1.0$ eV and $\Gamma_{AlAsSb} - \Gamma_{InGaAs} \sim 1.6$ eV),[7,8] has been proposed as a barrier layer for InGaAs channel MOSFETs.[9,10] Once the gate length is scaled to below 10 nm, thinner (3–5 nm) channels are required to maintain strong electrostatic gate control and mitigate short channel effects. However, thinning the InGaAs channel raises the eigen-state energy in the InGaAs well above the InGaAs conduction-band edge. When the transistor is turned on and $\sim 2.5 \times 10^{12}$ cm^{-2} carriers are introduced into the channel, the Fermi energy is in turn raised ~0.15 eV above the eigen-state energy. Given that the commonly reported $In_{0.52}Al_{0.48}As$ barrier offers only 0.52 eV conduction band offset to the $In_{0.53}Ga_{0.47}As$ channel,[11] this small conduction band offset is insufficient to fully confine electrons in the channel, in particular, for very narrow quantum wells with high eigen-state energy. Under such conditions, the bound state wavefunction extends significantly into the barriers, both increasing the transport effective mass and degrading the transistor electrostatics. Further, if the Fermi level in the channel approaches the barriers' conduction-band energy, carriers can escape from the channel into the barriers, particularly in the heavily doped source, leading to increased off-state leakage.[10] Replacing the InAlAs barriers with AlAsSb barriers increases the conduction band-offset, thereby reducing the barrier leakage current, and allows increased carrier density in the quantum well without loss of quantum confinement.

The electron transport properties of lattice-matched $In_{0.53}Ga_{0.47}As/In_{0.52}Al_{0.48}As$ 2DEGs have been reported extensively in the literature.[12–14] In comparison, there are only a few reports of electron transport in the lattice-matched $In_{0.53}Ga_{0.47}As/AlAs_{0.56}Sb_{0.44}$ material system,[9,15] yet detailed investigation of this system is necessary if AlAsSb barriers are to be used in highly scaled InGaAs-channel field effect transistors.

In this paper, we report the growth and electron transport properties in $In_{0.53}Ga_{0.47}As/AlAs_{0.56}Sb_{0.44}$ quantum well 2DEGs with a remote Si-doped $In_{0.52}Al_{0.48}As$ modulation-doped layer. InGaAs/AlAsSb 2DEGs with varying InGaAs quantum well thickness were grown and their properties were compared with that of $In_{0.53}Ga_{0.47}As/In_{0.52}Al_{0.48}As$ 2DEGs. The electron transport in quantum wells was then modeled based on the relaxation time approximation to examine the contribution of each scattering mechanism. Upon reducing the InGaAs channel thickness, stronger interface roughness scattering from InGaAs/AlAsSb interfaces degrades the electron mobility rapidly. Growth interruptions under either As or Sb exposure at the InGaAs/AlAsSb interfaces were investigated as a possible means to improve 2DEG mobility. It was observed that the 2DEG mobility for a 5 nm quantum well is independent of the selective group-V species exposure at the InGaAs/AlAsSb interfaces. By inserting a 2 ML(~0.5 nm) InAlAs layer at the InGaAs/AlAsSb interfaces, the interface scattering could be reduced and the 2DEG mobility of a 3 nm thick InGaAs/AlAsSb quantum well was improved from 1.63×10^3 $cm^2/V{\cdot}s$ to 2.71×10^3 $cm^2/V{\cdot}s$.

a)Electronic mail: cyhuang@ece.ucsb.edu

 © 2014 AIP Publishing LLC

[This article is copyrighted as indicated in the article. Reuse of AIP content is subject to the terms at: http://scitation.aip.org/termsconditions. Downloaded to] IP: 222.29.50.29 On: Tue, 20 May 2014 21:31:30

II. EXPERIMENTS

The lattice-matched $In_{0.53}Ga_{0.47}As/AlAs_{0.56}Sb_{0.44}$ 2DEG structures were grown on semi-insulating InP substrates by a Veeco GEN II solid source molecular beam epitaxy (SSMBE) system. The InGaAs/AlAsSb 2DEG structures consist of a semi-insulating InP substrate, a 270 nm non-intentionally doped (N.I.D) InAlAs buffer layer, a 30 nm N.I.D AlAsSb bottom barrier, a N.I.D InGaAs channel (3, 5, 7.5, or 10 nm thickness), a 3 nm N.I.D. AlAsSb spacer layer, a 3 nm $1.3 \times 10^{19}\,cm^{-3}$ Si-doped InAlAs modulation-doped layer, a 15 nm N.I.D AlAsSb top barrier and a 5 nm N.I.D InGaAs capping layer. For comparison, similar $In_{0.53}Ga_{0.47}As/In_{0.52}Al_{0.48}As$ 2DEGs were also grown; in these, the AlAsSb bottom barrier, the spacer layer, and the top barrier are replaced with N.I.D InAlAs layers. The non-intentionally doped impurity concentrations of InAlAs layers and AlAsSb layers were estimated to be around $10^{15}\,cm^{-3}$ and below $10^{15}\,cm^{-3}$, respectively. The 2DEG structures are shown in Figure 1(a). All layers were grown at 490 °C, as measured by an infrared pyrometer. The group-V species, As_2 and Sb_2, provided from As and Sb valved crackers, respectively, were used to grow $AlAs_{0.56}Sb_{0.44}$ layers with an As/Sb beam equivalent pressure ratio of around 5.1 and a total (As + Sb)/III ratio of around 22. After growing the AlAsSb bottom barrier, the group-III shutters were closed, interrupting growth for 30 s. During this interruption, the wafer was exposed to either an As or Sb column-V flux, with the As and Sb beam equivalent pressure (BEP) around 5.0×10^{-6} Torr and 1.0×10^{-7} Torr, respectively. After growing the InGaAs channel, the group-III shutters were closed, interrupting growth for 120 s. For some samples, during this interruption, the wafer was exposed to an As flux for 90 s and subsequently exposed to an Sb flux for 30 s. For other samples, the wafer was exposed to an As flux for 120 s. During this interruption, the As and Sb BEP were about 5.1×10^{-7} Torr and 1.0×10^{-7} Torr, respectively. From the XRD characterization of bulk AlAsSb layers, the lattice mismatch of AlAsSb barriers to InP is less than 0.5% and the full-width at half-maximum (FWHM) of AlAsSb peak was comparable to that of InAlAs layers with similar thickness, indicating a good control on the AlAsSb growth.[9]

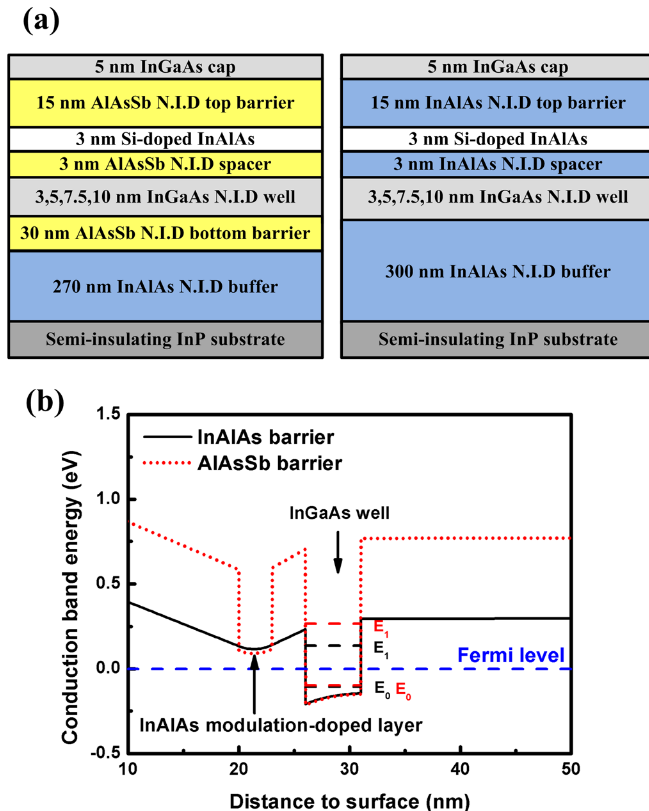

FIG. 1. (a) The InGaAs/AlAsSb and InGaAs/InAlAs 2DEG quantum well layer structures using modulation-doped InAlAs layers above the well. (b) Simulated conduction band profile for a 5 nm InGaAs well. The dashed lines indicate the Fermi level and the first two bound states band minima within the well.

Figure 1(b) shows the conduction band profile of a 5 nm InGaAs/AlAsSb 2DEG structure simulated by a 1-D self-consistent Schrödinger-Poisson simulation program. The conduction band energy of the AlAsSb barrier is linearly interpolated from the unstrained AlAs and AlSb materials, neglecting the bowing parameter. To measure the carrier concentration and carrier mobility of InGaAs/InAlAs and InGaAs/AlAsSb 2DEGs, the room temperature Hall effect measurements were carried out using van der Pauw technique with DC current at various magnetic fields of 0.2, 0.4, and 0.6 T. The variations of 2DEG mobility across the wafer were less than 10% for all the samples. The temperature-dependent Hall-effect measurements were measured from 45 K to room temperature in a magnetic field of 0.6 T.

III. TRANSPORT SCATTERING MODEL

In this section, we describe the electron transport models used to calculate electron mobility in the InGaAs quantum well. At low electric fields, the electron velocity is proportional to the electron mobility, which is associated with the electron effective mass and the electron scattering time. Scattering mechanisms including acoustic phonon scattering,[16] polar optical phonon scattering,[17,18] remote impurity scattering,[19] interface roughness scattering,[19] and alloy scattering[20] were considered in the calculations. The InGaAs quantum well was modeled with infinite barriers. This approximation is satisfactory because the AlAsSb barriers have a high conduction band offset to InGaAs wells. Further, only intra-valley scattering in the lowest sub-band was included. The inter-subband scattering is negligible since electrons mainly populate the first lowest subband, as seen in Figure 1(b). Electron-electron interaction and nonparabolic conduction band dispersion were not considered in the calculations.

A. Acoustic phonon scattering

Assuming no intersubband scattering in the quantum well, the scattering time for the acoustic phonon depends on the deformation-potential of the acoustic phonon in the crystal. The scattering time can be expressed as[16]

$$\frac{1}{\tau_{AC}} = \frac{3 m_n k_B T}{2\hbar^3 L} \frac{D^2}{\rho {\mu_L}^2}, \tag{1}$$

where D is the acoustic phonon deformation potential, ρ the InGaAs mass density, μ_L the longitudinal acoustic phonon

[This article is copyrighted as indicated in the article. Reuse of AIP content is subject to the terms at: http://scitation.aip.org/termsconditions. Downloaded to] IP: 222.29.50.29 On: Tue, 20 May 2014 21:31:30

velocity, m_n the electron effective mass, T the temperature, and L the well thickness.

B. Polar optical phonon scattering

Considering the electron scattering by the absorption of polar optical phonons in a narrow quantum well, the scattering time is approximated by Price and Ridley[17,18] as

$$\frac{1}{\tau_{PO}} = \frac{e^2 k_0}{8\hbar\kappa^*}\frac{1}{\exp[\hbar\omega_0/k_B T] - 1}, \quad (2)$$

where ω_0 is the optical phonon frequency, $k_0 = \sqrt{2m_n\omega_0/\hbar}$ the change of electron wave vector by phonon scattering, $(\kappa^*)^{-1} = {\kappa_\infty}^{-1} - {\kappa_0}^{-1}$, and κ_∞ and κ_0 are the high-frequency and low-frequency dielectric constants.

C. Remote impurity scattering

Following the treatment by Gold,[19] considering two dimensional sheet charges from modulation-doped impurities N_i at locations z_i from the bottom boundary of the InGaAs well, the scattering time for remote impurity scattering can be expressed as,

$$\frac{1}{\tau_{IM}} = \frac{1}{2\pi\hbar E_f}\int_0^{2k_f}\frac{\langle|U_{IM}|^2\rangle}{\varepsilon(q)^2}\frac{q^2}{({4k_f}^2 - q^2)^{1/2}}dq, \quad (3)$$

where E_f is the Fermi energy, $k_f = \sqrt{2\pi N_s}$ the Fermi wave vector, N_s the 2DEG sheet carrier density, $\varepsilon(q)$ the static dielectric function including screening effect by the two dimensional electron gas, and $\langle|U_{IM}|^2\rangle$ is the Coulomb scattering potential,

$$\langle|U_{IM}(q)|^2\rangle = N_i\left(\frac{e^2}{2\kappa_0 q}\right)^2 \times F(q,z_i)^2, \quad (4)$$

κ_0 is the dielectric constant of the InGaAs well, and the form factor $F(q,z_i)$is[19]

$$F(q,z_i) = \frac{8\pi^2}{Lq}\frac{1}{4\pi^2 + L^2q^2}\frac{1}{2}\exp(-q(z_i - L))[1 - \exp(-qL)]. \quad (5)$$

In this calculation, the Thomas-Fermi approximation for two dimensional electron gas was used, and the static dielectric function was approximated as $\varepsilon(q) = 1 + q_{TF}/q$, where $q_{TF} = 2/a_B$ and a_B is the Bohr radius.

D. Interface roughness scattering

Interface roughness scattering is well-known to be the dominant scattering event in thin quantum wells.[21,22] The interface roughness can be considered as the variation in the well thickness, leading to a broadening subband energy in the quantum well. Again, following the treatment of Gold,[19] the interface topology is assumed as a Gaussian fluctuation with the average height Δ and the correlation length Λ expressed as

$$\left\langle\Delta(\vec{r})\Delta(\vec{r}')\right\rangle = \Delta^2\exp\left(-\frac{|\vec{r} - \vec{r}'|^2}{\Lambda^2}\right), \quad (6)$$

where we assume that the top and bottom interfaces are described by the same parameters. The scattering potential $\langle|U_{IF}(q)|^2\rangle$ of the interface roughness scattering is

$$\langle|U_{IF}(q)|^2\rangle = 2\left(\frac{4\pi}{L^2}\right)\left(\frac{\pi}{k_F L}\right)^4(E_f\Delta\Lambda)^2\exp\left(-\frac{q^2\Lambda^2}{4}\right), \quad (7)$$

while the momentum relaxation time is

$$\frac{1}{\tau_{IF}} = \frac{1}{2\pi\hbar E_f}\int_0^{2k_f}\frac{\langle|U_{IF}|^2\rangle}{\varepsilon(q)^2}\frac{q^2}{({4k_f}^2 - q^2)^{1/2}}dq. \quad (8)$$

E. Alloy scattering

Given that $In_xGa_{1-x}As$ is a ternary alloy, alloy scattering caused by the random distribution of group-III elements also significantly affects mobility.[20] For an infinite quantum well, the electron mobility limited by alloy scattering is[20]

$$\mu_{Alloy} = \frac{128Le\hbar^3}{27\pi^2{m_n}^2\Omega x(1-x)|\Delta U|^2}, \quad (9)$$

where Ω is the volume of the primitive cell, x the alloy composition, and ΔU the alloy scattering potential. It is worth noting that the electron mobility limited by alloy scattering decreases as the well thickness L decreases, and is independent of temperature.

F. Total mobility

The total electron mobility contributed by each individual scattering mechanism is determined by Matthiessen's rule,

$$\frac{1}{\mu_{Total}} = \frac{1}{\mu_{AC}} + \frac{1}{\mu_{PO}} + \frac{1}{\mu_{IM}} + \frac{1}{\mu_{IF}} + \frac{1}{\mu_{Alloy}}, \quad (10)$$

with $\mu_j = e\tau_j/m_n$ and τ_j is the scattering time defined by each scattering mechanism. Table I summarizes the material parameters used in the calculations. Since we have no experimental measurement of the interface roughness parameters of these 2DEGs samples, we assumed the average height Δ is 2.93 Å (1 monolayer) and adjusted the correlation length $\Lambda \sim 210$ Å to obtain the best fit between calculated and measured mobilities of a narrow (3 nm) quantum well. In addition, an alloy scattering potential ΔU of 0.7 eV was determined by a best fit between theory and experiment of the 7.5 nm and 10 nm thick quantum well samples. This value is comparable to that of previously reported InGaAs/InAlAs heterostructures.[14,20,23]

IV. RESULTS AND DISCUSSION

Figure 2 shows a comparison between calculated and measured temperature-dependent Hall mobility for InGaAs/AlAsSb 2DEGs with 3 nm, 5 nm, 7.5 nm, and 10 nm well thickness. The 2DEG carrier concentration for all the samples in Figure 2 is c.a. 2.0–2.5 × 10^{12} cm^{-2}, and is

[This article is copyrighted as indicated in the article. Reuse of AIP content is subject to the terms at: http://scitation.aip.org/termsconditions. Downloaded to] IP: 222.29.50.29 On: Tue, 20 May 2014 21:31:30

TABLE I. Material parameters used in the calculations of the InGaAs/AlAsSb 2DEG mobility.

Electron effective mass density	m_n	$0.041\ m_0$
2DEG carrier concentration	N_s	$2.4 \times 10^{12}\,\text{cm}^{-2}$
Impurity concentration	N_i	$3.9 \times 10^{12}\,\text{cm}^{-2}$
Deformation potential	D	9.4 eV
Alloy scattering potential	ΔU	0.7 eV
InGaAs DC dielectric constant	κ_0	$13.9\ \varepsilon_0$
High-frequency dielectric constant	κ_∞	$11.5\ \varepsilon_0$
LO phonon energy of InGaAs	ω_0	34.5 meV
LA phonon velocity	μ_L	$4253\,\text{ms}^{-1}$
Mass density of InGaAs	ρ	$5690\,\text{kg/m}^3$
Interface average height	Δ	2.93 Å
Interface correlation length	Λ	210 Å

insensitive to temperature, varying by less than ±5% between 45 K and 300 K. Noting again that the correlation length has been adjusted to obtain best fit, the theoretical calculations show good agreement with the experimental data. For thick quantum wells (10 nm and 7.5 nm), the room temperature mobility is dominated by polar optical phonon scattering, while the low temperature mobility is primarily dominated by alloy scattering in the channel. In contrast, for a 5 nm thick well, the low temperature mobility is dominated by the combination of interface roughness and alloy scattering, with polar optical phonons also significantly contributing to the net scattering rate at 300 K. Further shrinking the well thickness to 3 nm, the interface roughness scattering becomes dominant at all temperatures.

Figure 3 compares simulation and measurements of 2DEG electron mobility versus InGaAs well thickness at 45 K and 300 K. For thicker wells ($L > 10$ nm), the 2DEG mobility is limited primarily by alloy scattering at 45 K and by polar optical phonon scattering at 300 K. For thinner wells, interface roughness scattering increases and becomes the limiting scattering mechanism for wells thinner than 4 nm. Since the interface roughness scattering is independent of temperature, the room temperature 2DEG mobility for thin wells is also degraded by the strong interface roughness scattering. As seen in Eq. (7), the scattering potential of interface roughness scattering $\langle |U_{IF}(q)|^2 \rangle$ is proportional to the inverse sixth power of the well thickness (L^{-6}). Hence, for the thinner wells, the electron mobility decreases dramatically as the well is made thinner.

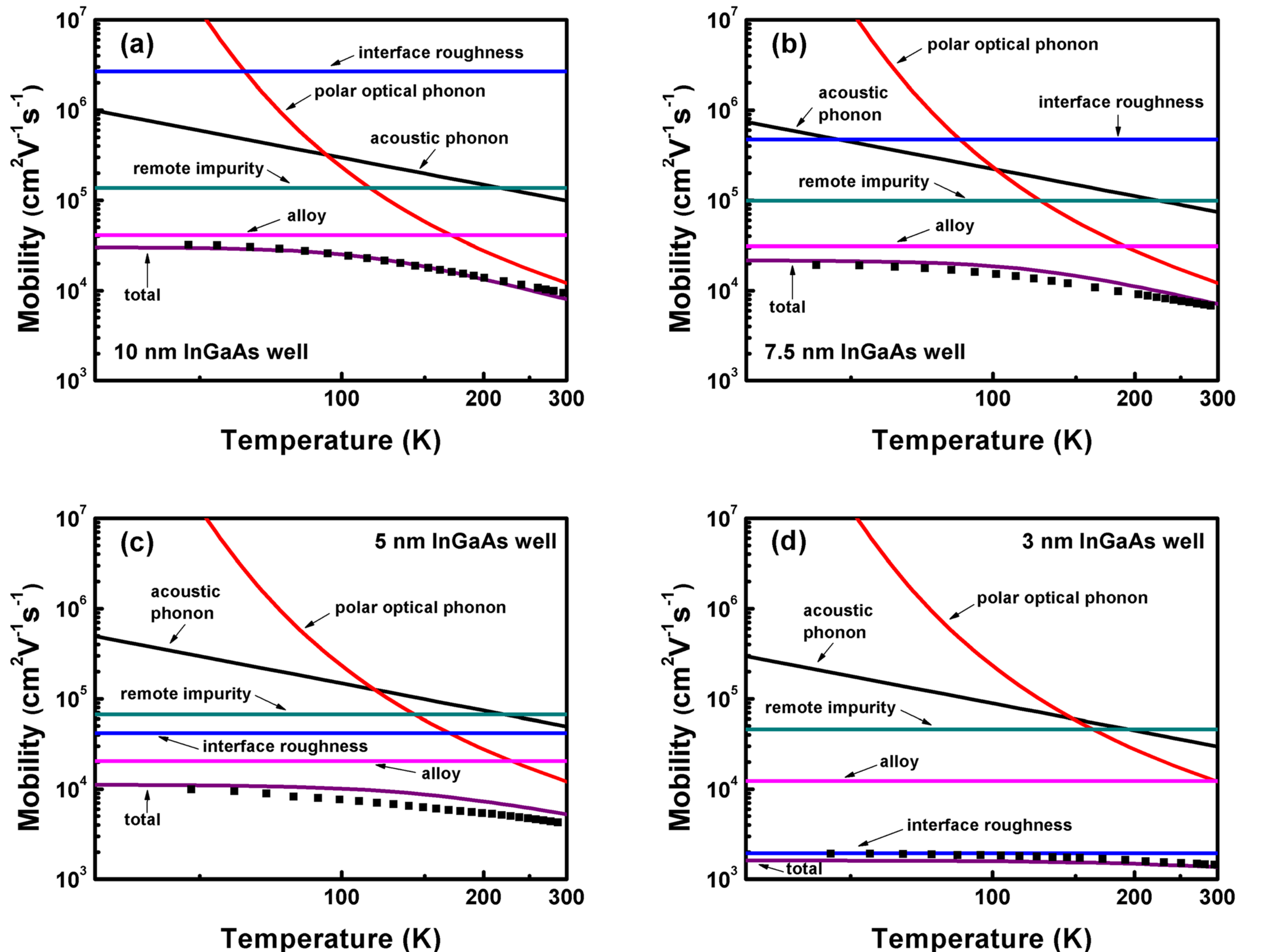

FIG. 2. Measured temperature-dependent Hall mobilities and the corresponding numerical calculations of mobilities for 10 nm, 7.5 nm, 5 nm, and 3 nm thick InGaAs/AlAsSb 2DEGs. The material parameters used in the calculations are shown in Table I.

[This article is copyrighted as indicated in the article. Reuse of AIP content is subject to the terms at: http://scitation.aip.org/termsconditions. Downloaded to] IP: 222.29.50.29 On: Tue, 20 May 2014 21:31:30

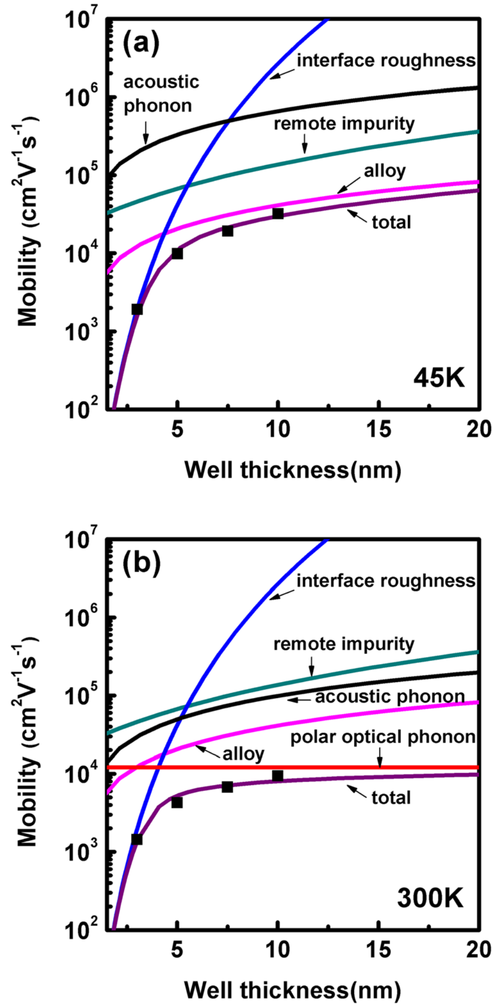

FIG. 3. Measured and calculated (a) low temperature (45 K) and (b) room temperature (300 K) Hall mobilities of InGaAs/AlAsSb 2DEGs as a function of InGaAs quantum well thickness.

Figure 4 compares the measured room temperature and low temperature Hall mobility of InGaAs/InAlAs and InGaAs/AlAsSb 2DEGs as a function of well thickness. The

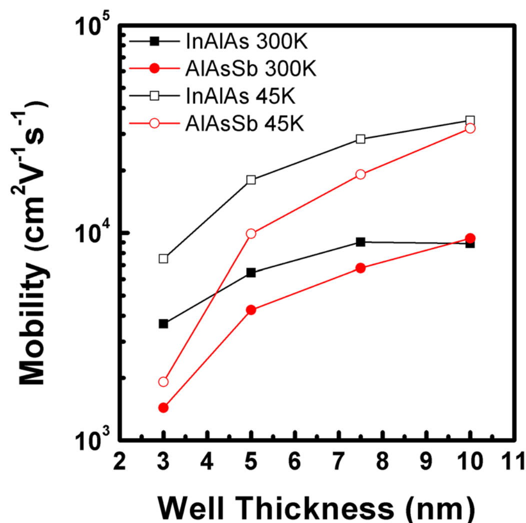

FIG. 4. Measured low temperature (45 K) and room temperature (300 K) mobilities of InGaAs/InAlAs and InGaAs/AlAsSb 2DEGs as a function of the InGaAs well thickness.

2DEG mobility is found to be comparable for both InAlAs and AlAsSb barriers for thick (10 nm) InGaAs quantum wells. However, upon reducing the quantum well thickness, the 2DEG mobility for both InGaAs/InAlAs and InGaAs/AlAsSb heterostructures decreases significantly, with a particularly strong degradation for the InGaAs/AlAsSb 2DEGs. This result indicates that interface roughness scattering is stronger for InGaAs/AlAsSb interfaces than for InGaAs/InAlAs interfaces. The larger interface roughness scattering of the InGaAs/AlAsSb interfaces could be attributed to two mechanisms: First, the larger conduction band offset at the InGaAs/AlAsSb heterojunction results in a large fluctuation of the bound state energy in the InGaAs well for a given fluctuation in well thickness, leading to stronger intrasubband scattering than for an InGaAs/InAlAs heterojunction.[24] Second, as reported in Refs. 22, 25, and 26, given the higher aluminum content of an AlAsSb bottom barrier than of an InAlAs bottom barrier, greater surface roughness may arise at this interface either due to the proclivity of high aluminum content surfaces to oxidize,[27] or due to impurities in the MBE system's aluminum source.[28]

Given the evidence presented above that interface roughness scattering is responsible for the observed degradation of 2DEG mobility in thin quantum wells, treatment of the interfaces is critical for further improvement on 2DEG mobility in 3–5 nm quantum wells. For this purpose, different interface treatments including As exposure and Sb exposure at the InGaAs/AlAsSb interfaces were investigated. Tuttle *et al.*[29] reported that the 2DEG mobility in InAs/AlSb quantum wells was strongly dependent on the growth of the InAs/AlSb interfaces, with InSb-like interfaces providing significantly higher 2DEG mobility than AlAs-like interfaces. The difference was attributed to the scattering between transport electrons and antisite defects created at the AlAs-like interfaces. Following the similar concept, we therefore treated the InGaAs/AlAsSb interfaces with different group-V species. Since the complexity of InGaAs/AlAsSb interfaces leads to six combinations of interface (InAs, InSb, GaAs, GaSb, AlAs, and AlSb), instead of intentionally growing a certain type of interface by the shutter sequences during MBE growth, as described earlier, we interrupted the growth and exposed the surface to As or Sb for at least 30 s. Table II summarizes the Hall results of various 2DEG samples. It could be found that for narrow wells (5 nm) under this investigation, the room temperature 2DEG mobility is insensitive to which group-V species (As or Sb) the wafer was exposed

TABLE II. InGaAs/AlAsSb 2DEG Hall mobility as a function of column-V exposure during growth interruptions at the InGaAs/AlAsSb interfaces.

	Column-V exposure during interruption			
Well thickness (nm)	Top interface	Bottom interface	N_s, 300 K (10^{12} cm^{-2})	μ, 300 K (10^3 cm^2/V·s)
5	As	As	2.30	4.95
5	As	Sb	2.36	4.90
5	Sb	As	2.30	4.88
5	Sb	Sb	2.23	4.87

[This article is copyrighted as indicated in the article. Reuse of AIP content is subject to the terms at: http://scitation.aip.org/termsconditions. Downloaded to] IP: 222.29.50.29 On: Tue, 20 May 2014 21:31:30

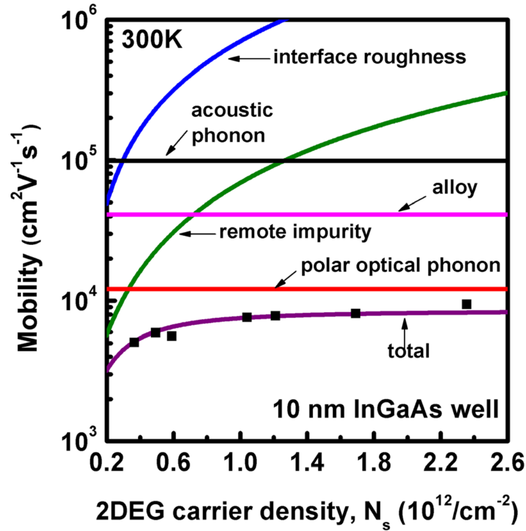

FIG. 5. Measured and calculated room temperature mobilities of InGaAs/AlAsSb 2DEGs as a function of 2DEG carrier concentration (Ns). The modulation-doped impurity concentration was varied from 1.0×10^{12} to $3.9 \times 10^{12}\,\mathrm{cm}^{-2}$ by controlling the Si shutter opening time or the Si cell temperature. The calculation assumes the modulation-doped impurity concentration, N_i, is $2 \times 10^{12}\,\mathrm{cm}^{-2}$.

to during the growth interruptions at the InGaAs/AlAsSb interfaces. Another sample with 2 min Sb interruption at both the top interface and the bottom interface, and the other sample with an intentionally grown 1.25 monolayer InSb-like interface (with the similar shutter sequences described in Ref. 29), both showed similar carrier concentration and room temperature 2DEG mobility as the samples in Table II.

The dependence of mobility on carrier concentration was also investigated. A series of 10 nm thick InGaAs/AlAsSb quantum wells with varying modulation-doped 2D carrier concentrations were grown and characterized. Figure 5 compares measured and calculated room temperature mobility as a function of 2DEG carrier concentration. The 2DEG carrier concentration in the 10 nm InGaAs quantum well is well-controlled by varying the modulation-doped concentration in the barrier (Figure 5), which indicates that the density of defects either in the AlAsSb barriers or at the InGaAs/AlAsSb interfaces is negligible compared to the 2DEG carrier concentrations typical of field-effect transistors. Furthermore (Figure 5), alloy scattering, acoustic phonon scattering, and polar optical phonon scattering are independent of 2DEG carrier concentration. The room temperature mobility in the 10 nm well is primarily limited by polar optical phonon scattering. For 2DEG carrier concentrations less than $3 \times 10^{11}\,\mathrm{cm}^{-2}$, remote impurity scattering from the modulation-doped layer becomes the dominant scattering mechanism. Remote impurity scattering can be reduced by increasing the distance between the modulation doping and the quantum well.

Given that InGaAs/InAlAs heterointerfaces provide lower interface roughness scattering than InGaAs/AlAsSb heterointerfaces, we then grew InGaAs/AlAsSb quantum wells with a 5 Å (~2ML) InAlAs layer inserted at the InGaAs/AlAsSb interfaces. Table III summarizes the room temperature mobility of 3 nm and 5 nm thick quantum wells with and without the InAlAs interfacial layer. With a 2ML InAlAs interfacial layer, the 2DEG mobility for the 3 nm thick InGaAs well increases from $1.63 \times 10^3\,\mathrm{cm}^2$/V·s to $2.71 \times 10^3\,\mathrm{cm}^2$/V·s, while the mobility for the 5 nm thick InGaAs well increases from $4.78 \times 10^3\,\mathrm{cm}^2$/V·s to $5.69 \times 10^3\,\mathrm{cm}^2$/V·s.

TABLE III. Comparison of InGaAs/AlAsSb 2DEG Hall mobility with As interruption and with an insertion of two monolayer InAlAs at the InGaAs/AlAsSb heterointerfaces.

Well thickness (nm)	Top interface	Bottom interface	N_s, 300 K ($10^{12}\,\mathrm{cm}^{-2}$)	μ, 300 K ($10^3\,\mathrm{cm}^2$/V·s)
5	As	As	2.13	4.78
5	2ML InAlAs	2ML InAlAs	1.94	5.69
3	As	As	1.89	1.63
3	2ML InAlAs	2ML InAlAs	1.84	2.71

Note that the Hall mobility of InGaAs/AlAsSb 2DEGs with the 2ML InAlAs interfacial layers is still inferior to that of InGaAs/InAlAs 2DEGs ($\mu \sim 3.65 \times 10^3\,\mathrm{cm}^2$/V·s for a 3 nm well and $\mu \sim 6.43 \times 10^3\,\mathrm{cm}^2$/V·s for a 5 nm well). Further, Ref. 30 reports a 2DEG mobility of ~4200 cm^2/V·s at 4 K in a 2.3 nm thick InGaAs quantum well with InP barriers. Given the smaller barrier energies associated with the InGaAs/InAlAs (~0.5 eV) and InGaAs/InP interfaces (~0.2 eV), these high mobilities may in part result from the reduced interface roughness scattering associated with the weaker quantum confinement in these materials systems.

V. CONCLUSIONS

We report the growth and the electron transport in InGaAs/AlAsSb 2DEGs and compare the mobility with that of InGaAs/InAlAs 2DEGs. Room temperature mobility up to $9 \times 10^3\,\mathrm{cm}^2$/V·s was demonstrated in InGaAs/AlAsSb quantum wells, a mobility comparable to that of InGaAs/InAlAs wells. For well thicknesses below 4 nm, interface roughness scattering becomes the dominant scattering mechanism, limiting the 2DEG mobility at low temperature and degrading the room temperature mobility. Stronger interface roughness scattering is observed for InGaAs/AlAsSb heterointerfaces than for InGaAs/InAlAs heterointerfaces. The InGaAs/AlAsSb 2DEGs mobility for 5 nm wells is independent of the group-V species exposure during growth interruptions at the InGaAs/AlAsSb interfaces. Adding 2ML InAlAs interfacial layers at the InGaAs/AlAsSb interfaces reduces the interface roughness scattering and increases the 2DEG mobility of a 3 nm thick InGaAs well from $1.63 \times 10^3\,\mathrm{cm}^2$/V·s to $2.71 \times 10^3\,\mathrm{cm}^2$/V·s.

ACKNOWLEDGMENTS

The authors gratefully acknowledge support from the Semiconductor Research Corporation through the Nonclassical CMOS Research Center (Task ID 1437.009). C. Y. Huang thanks John English for his assistance with MBE growth. Work made use of the NNIN National Nanofabrication facilities and the MRL Shared Experimental

[This article is copyrighted as indicated in the article. Reuse of AIP content is subject to the terms at: http://scitation.aip.org/termsconditions. Downloaded to] IP: 222.29.50.29 On: Tue, 20 May 2014 21:31:30

Facilities supported by the MRSEC Program of the National Science Foundation under Award No. DMR-1121053. The authors thank W. Frensley (U.T. Dallas) for providing the Schrödinger-Poisson solver.

[1]M. Radosavljevic, B. Chu-Kung, S. Corcoran, G. Dewey, M. K. Hudait, J. M. Fastenau, J. Kavalieros, W. K. Liu, D. Lubyshev, M. Metz, K. Millard, N. Mukherjee, W. Rachmady, U. Shah, and R. Chau, in *International Electron Devices Meeting* (2009), p. 319.
[2]D.-H. Kim, J. A. del Alamo, D. A. Antoniadis, J. Li, J.-M. Kuo, P. Pinsukanjana, Y.-C. Kao, P. Chen, A. Papavasiliou, C. King, E. Regan, M. Urteaga, B. Brar, and T.-W. Kim, Appl. Phys. Lett. **101**, 223507 (2012).
[3]J. A. del Alamo, Nature **479**, 317 (2011).
[4]J. J. Gu, X. W. Wang, H. Wu, J. Shao, A. T. Neal, M. J. Manfra, R. G. Gordon, and P. D. Ye, in *International Electron Devices Meeting* (2012), p. 633.
[5]M. Egard, L. Ohlsson, B. M. Borg, F. Lenrick, R. Wallenberg, L.-E. Wernersson, and E. Lind, in *International Electron Devices Meeting* (2011), p. 303.
[6]S. Lee, C. Y. Huang, D. C. Elias, J. J. M. Law, V. Chobpattana, S. Krämer, B. J. Thibeault, W. Mitchell, S. Stemmer, A. C. Gossard, and M. J. W. Rodwell, Appl. Phys. Lett. **103**, 233503 (2013).
[7]Y. Nakata, Y. Sugiyama, T. Inata, O. Ueda, S. Sasa, S. Muto, and T. Fujii, MRS Proceedings **198**, 289 (1990).
[8]N. Georgiev and T. Mozume, J. Appl. Phys. **89**, 1064 (2001).
[9]C. Y. Huang, J. J. M. Law, H. Lu, M. J. W. Rodwell, and A. C. Gossard, in *MRS Online Proceedings Library* (2013), p. 1561, mrss13-1561-cc01-10.
[10]C. Y. Haung, S. Lee, D. Cohen-Elias, J. J. M. Law, A. D. Carter, V. Chobpattana, S. Stemmer, A. C. Gossard, and M. J. W. Rodwell, Appl. Phys. Lett. **103**, 203502 (2013).
[11]I. Vurgaftman, J. R. Meyer, and L. R. Ram-Mohan, J. Appl. Phys. **89**, 5815 (2001).
[12]A. Kastalsky, R. Dingle, K. Y. Cheng, and A. Y. Cho, Appl. Phys. Lett **41**, 274 (1982).
[13]W. Walukiewicz, H. E. Ruda, J. Lagowski, and H. C. Gatos, Phys. Rev. B **30**, 4571 (1984).
[14]T. Matsuoka, E. Kobayashi, K. Taniguchi, C. Hamaguchi, and S. Sasa, Jpn. J. Appl. Phys., Part 1 **29**, 2017 (1990).
[15]M. Ahoujja, S. Elhamri, R. S. Newrock, D. B. Mast, W. C. Mitchel, I. Lo, and A. Fathimulla, J. Appl. Phys. **81**, 1609 (1997).
[16]V. K. Arora and A. Naeem, Phys. Rev. B **31**, 3887 (1985).
[17]P. J. Price, Ann. Phys. **133**, 217 (1981).
[18]B. K. Ridley, J. Phys. C: Solid State Phys. **15**, 5899 (1982).
[19]A. Gold, Phys. Rev. B **35**, 723 (1987).
[20]D. Chattopadhyay, Phys. Rev. B **31**, 1145 (1985).
[21]H. Sakaki, T. Noda, K. Hirakawa, M. Tanaka, and T. Matsusue, Appl. Phys. Lett. **51**, 1934 (1987).
[22]C. R. Bolognesi, H. Kroermer, and J. H. English, Appl. Phys. Lett. **61**, 213 (1992).
[23]D. Chattopadhyay, Phys. Rev. B **38**, 13429 (1988).
[24]J. M. Li, J. J. Wu, X. X. Han, Y. W. Lu, X. L. Liu, Q. S. Zhu, and Z. G. Wang, Semicond. Sci. Technol. **20**, 1207 (2005).
[25]N. Ikarashi, M. Tanaka, H. Sakaki, and K. Ishida, Appl. Phys. Lett. **60**, 1360 (1992).
[26]P. M. Petroff, R. C. Miller, A. C. Gossard, and W. Wiegmann, Appl. Phys. Lett. **44**, 217 (1984).
[27]D. E. Wohlert, K. L. Chang, H. C. Lin, K. C. Hsieh, and K. Y. Cheng, J. Vac. Sci. Technol. B **18**, 1590 (2000).
[28]N. Chand and S. N. G. Chu, Appl. Phys. Lett **57**, 1796 (1990).
[29]G. Tuttle, H. Kroemer, and J. H. English, J. Appl. Phys. **67**, 3032 (1990).
[30]D. Schneider, L. Elbrecht, J. Creutzburg, A. Schlachetzki, and G. Zwinge, J. Appl. Phys. **77**, 2828 (1995).

[This article is copyrighted as indicated in the article. Reuse of AIP content is subject to the terms at: http://scitation.aip.org/termsconditions. Downloaded to] IP: 222.29.50.29 On: Tue, 20 May 2014 21:31:30